

1
2
3
4
5
6 **Diagnosing the influence of a receding snow boundary on simulated midlatitude cyclones**
7 **using piecewise potential vorticity inversion**
8

9
10 *By*
11

12
13 **Corresponding Author:** Melissa L. Breeden, NOAA Earth System Research Laboratory,
14 Chemical Sciences Division, Boulder CO
15

16
17 Ryan Clare, Naval Research Laboratory, Monterey, CA
18

19
20 Jonathan E. Martin, Department of Atmospheric and Oceanic Sciences, University of
21 Wisconsin-Madison, Madison, WI
22

23
24 Ankur R. Desai, Department of Atmospheric and Oceanic Sciences, University of
25 Wisconsin-Madison, Madison, WI
26
27
28
29
30
31
32
33
34
35
36
37
38
39
40
41
42
43
44
45
46

47 **Abstract:** Previous research has found a relationship between the equatorward extent of
48 snow cover and low-level baroclinicity, suggesting a link between the development and
49 trajectory of midlatitude cyclones and the extent of preexisting snow cover. Midlatitude cyclones
50 are more frequent 50-350 km south of the snow boundary, coincident with weak maxima in the
51 environmental Eady growth rate. The snow line is projected to recede poleward with increasing
52 greenhouse gas emissions, possibly affecting the development and track of midlatitude cyclones
53 during Northern Hemisphere winter. Detailed examination of the physical implications of a
54 modified snow boundary on the lifecycle of individual storms has, to date, not been undertaken.
55 The present study investigates the impact of a receding snow boundary on two cyclogenesis
56 events using Weather Research and Forecasting (WRF) model simulations initialized with
57 observed and projected future changes to snow extent as a surface boundary condition. Potential
58 vorticity diagnosis of the modified cyclone simulations isolates how changes in surface
59 temperature, static stability, and relative vorticity arising from the altered boundary affect the
60 developing cyclone. We find that the surface warm anomaly associated with snow removal
61 lowered heights near the center of the two cyclones investigated, strengthening their cyclonic
62 circulation. However, the direct effect of snow removal is mitigated by the stability response and
63 an indirect relative vorticity response to snow removal. Due to these opposing effects, it is
64 suggested that the immediate effect of receding snow cover on midlatitude cyclones is likely
65 minimal and depends on the stage of the cyclone lifecycle.

66
67

1. Introduction

68 As the planet warms, the climatological southern edge of snow cover during boreal winter
69 and spring is projected to move poleward (Manabe and Wetherald 1980; Brown 2000; Lemke et
70 al. 2007; Gan et al. 2013). Rydzik and Desai (2014) found that there was a statistical relationship
71 between the location of the snow boundary, low-level baroclinicity, and cyclone tracks,
72 presumably related to enhanced radiative, thermal, and moisture gradients along the snow line.
73 Consequently, it is possible that changes in the snow boundary could impact aspects of
74 developing cyclones over the next century.

75 The large-scale, low-frequency circulation response to receding snow cover has been
76 investigated previously and is nonnegligible. Walsh and Ross (1986) used the National Center
77 for Atmospheric Research (NCAR) Community Forecast Model to force anomalous snow extent
78 over North America, which, months later, induced remote temperature responses over
79 Scandinavia and western Europe. Klingaman et al. (2008) examined the large-scale response to

80 anomalous Great Plains snow cover imposed in simulations using the Community Atmosphere
81 Model and found a response in Eurasian temperatures related to a positive North Atlantic
82 Oscillation (NAO) that developed at a lag of several months. Sobolowski et al. (2010) examined
83 the low-frequency, large-scale atmospheric response to a persistent snow cover anomaly using a
84 pair of 40-member atmospheric general circulation model simulations with high and low-snow
85 forcing, and also found a transient eddy response in the North Atlantic storm track due to
86 anomalous snow cover over North America.

87 A separate question that has also received research attention is -- what is the immediate (i.e.
88 occurring within days following production of a snow cover anomaly), regional atmospheric
89 response to snow cover? Using a one-dimensional snowpack model, Ellis and Leathers (1999)
90 simulated the effect of snow removal on four cold air masses that developed in the Great Plains
91 region of the United States. They found that for all four cases, the air masses warmed on average
92 by 6-10°C during the daytime, and by 1-2°C during nighttime, primarily through sensible heat
93 fluxes from the ground to the air mass. Elguindi et al. (2005) compared the intensity and sensible
94 weather associated with cyclogenesis in the Great Plains of North America for cases with the
95 observed snow boundary and for simulations with snow completely covering the model domain.
96 They found that covering the domain with snow led to weaker mean sea level pressure minima,
97 weaker fronts and thermal advection, and reduced precipitation and cloud cover due to weaker
98 vertical motion. Perhaps directly related to the former pair of attributes, increased static stability
99 of the lower troposphere was also characteristic of the snow-covered domain.

100 Previous research examining how a change in snow cover affects the development of
101 extratropical cyclones has focused on the presence of more-than-typical snow cover and colder
102 than normal temperatures. Whether the tropospheric response and influence on cyclones in the

103 *absence* of snow and *warmer* than normal temperatures produce an equal and opposite response
104 remains to be determined. In the present study, we have designed modeling experiments to test if
105 the removal of snow will affect the strength and/or trajectory of developing cyclones over North
106 America. The removal of snow is hypothesized to increase low-level temperature and
107 consequently reduce static stability. To isolate the direct and indirect effects snow removal has
108 on the circulation, we applied piecewise quasi-geostrophic potential vorticity (QGPV) inversion.
109 The inversion technique can isolate the geopotential height response to changes in a) surface
110 temperature, b) static stability, and c) relative vorticity, that arise due to the removal of snow. It
111 is reasonable to anticipate that the warm surface temperature anomaly associated with snow
112 removal, manifests itself as a cyclonic QGPV anomaly (Bretherton 1966), and as a result,
113 enhances the circulation of developing cyclones. Additionally, we suppose that the vertical
114 structure of the resultant surface warm anomaly will reduce the static stability of the environment
115 near the cyclone, which can enhance vertical motion, cloud cover and precipitation.

116 The paper is organized as follows. Section 2 describes both the modeling simulations
117 designed to test the immediate impact snow removal has on cyclogenesis as well as the potential
118 vorticity inversion technique used for analysis. Section 3 presents results from two selected
119 cases, including a synoptic overview and results from QGPV inversion. A discussion of results
120 and concluding remarks are offered in Section 4.

121 **2. Methodology**

122 To test the hypothesized influence of snow removal on cyclogenesis, a suite of model
123 simulations was designed that uses the observed snow boundary position (the control simulation)
124 and a range of plausible changes to the snow line as projected by climate models (see Clare et al.
125 (submitted) for more details). The difference in geopotential height between the control and

126 modified simulations was calculated throughout the troposphere for each case. The resultant
127 height anomaly fields were then used for piecewise potential vorticity inversion, to isolate and
128 quantify the direct and indirect effects, such as changes in temperature and static stability, the
129 modified snow boundary had on the circulation.

130 *2.1 Simulation Design*

131 We ran simulations using the Weather Research and Forecasting (WRF) model version
132 4.0.3 with 30 km grid spacing for 20 subjectively selected cyclone cases that occurred during
133 boreal winter (November – March). The domain for this study includes the continental United
134 States as well as much of Canada and Mexico and is centered over the Great Plains region.
135 Output from 14 models of the fifth phase of the Coupled Model Intercomparison Project
136 (CMIP5), using the representative concentration pathway (RCP) 4.5 and 8.5 scenarios, was used
137 to determine a range of possible modifications to the position of the snow boundary by the year
138 2100 that could arise from future changes in greenhouse gas concentrations. Each of the CMIP5
139 models used to determine the ranges of snow boundary retreat applied in this experiment are
140 present in the study of 22 CMIP5 models by Brutel-Vuilmet et al. (2013). They found that
141 though the models did not adequately capture significant long-term snow mass reductions in
142 spring, when ensemble-averaged, the models studied were able to realistically reproduce
143 observed snow water equivalent in the period from 1979-2005. Eight of those models were
144 ultimately excluded from consideration in this experiment as a result of restricted data
145 availability, resolution issues, or large regional biases. The remaining model simulations were
146 sorted based upon their projected changes to the snow boundary. For each simulation, the
147 monthly mean change in the snow line between the 2080-2099 and 1986-2005 periods was
148 determined. The projected changes were then grouped into 10th, 50th, and 90th percentile

149 categories for each month. For each of our selected cases, we ran simulations with each
150 percentile's poleward snow line retreat (10th, 50th, and 90th) applied to the observed snow
151 boundary, as well as a simulation with complete snow removal.

152 Additionally, simulations for each case and percentile of snow line retreat were initialized
153 at a range of 0 to 4 days prior to cyclogenesis at 24-hour intervals, ultimately yielding 500
154 distinct simulations. Information regarding the overall results of all simulations can be found in
155 Clare et al. (submitted). Here, two cyclogenesis cases were selected for in-depth analysis. We
156 chose to compare simulations of these cases initialized 4 days prior to cyclogenesis, and consider
157 differences between the control and 90th percentile simulations, to analyze the strongest response
158 to snow removal while remaining within the range of plausible future changes. Model output was
159 interpolated to pressure surfaces at 50 hPa intervals from 1000 – 100 hPa at 6-hourly temporal
160 resolution, and was regridded onto a 1°x1° latitude-longitude grid.

161 2.2 Anomaly Calculations

162 We use a potential vorticity inversion approach (described in Section 2.3) that employs
163 geopotential height on pressure surfaces to calculate and invert QGPV. To keep our view of the
164 cases consistent with the inversion framework, we consider the evolution of the surface cyclone
165 on pressure surfaces as well. Using each case's control simulation, the mean state, \bar{z} , was defined
166 as the 7-day average over which each selected cyclone developed, corresponding to 0000 UTC 3
167 March 2005 – 1800 UTC 9 March 2005 and 0000 UTC 22 January 1996 and 1800 UTC 28
168 January 1996. To track the geopotential height minimum associated with each surface cyclone,
169 we calculated geopotential height anomalies, $z' = z - \bar{z}$. The evolution of the surface cyclone
170 was then considered using the 1000 hPa z' fields in each case. To determine the change in the
171 height and temperature fields arising from the imposed retreat of the snow boundary, the control

172 simulation height fields were subtracted from those of the 90th percentile snow removal
 173 simulations: $z'' = z_{90} - z_{CTRL}$. Temperature anomalies due to removal of snow were calculated
 174 in the same manner: $T'' = T_{90} - T_{CTRL}$.

175 2.3 Quasi-Geostrophic Potential Vorticity Inversion

176 We used piecewise quasi-geostrophic potential vorticity (QGPV) inversion to test the
 177 hypothesized impact on the geopotential height field of the near-surface temperature anomaly
 178 created by removing snow. The QGPV approach is particularly amenable to the present analysis,
 179 as the components of QGPV linearly combine to produce the observed geopotential height field.
 180 QGPV is defined as the sum of the planetary vorticity, geostrophic relative vorticity, and a
 181 function of static stability:

$$182 \quad q = f + \frac{1}{f_0} \nabla^2 \phi + f_0 \frac{\partial}{\partial p} \left(\frac{1}{\sigma} \frac{\partial \phi}{\partial p} \right) \quad (1)$$

183 Where $\nabla^2 = \left(\frac{\partial^2}{\partial x^2}, \frac{\partial^2}{\partial y^2} \right)$, the two-dimensional Laplacian, ϕ represents deviations from the
 184 reference atmosphere geopotential, f is the Coriolis parameter, and σ is the reference atmosphere
 185 static stability ($\sigma = -\frac{\alpha}{\theta} \frac{d\theta}{dp}$), where α is specific volume. To investigate the changes in QGPV
 186 associated with a receding snow line, we calculated QGPV anomalies using the z'' and T'' fields
 187 for each case, and split the anomalies into contributions from relative vorticity and static stability
 188 (Eqns 2, 4). Horizontal variations in geopotential manifest themselves in the geostrophic relative
 189 vorticity term (Eqn 2), so that in the Northern Hemisphere cyclones are characterized by relative
 190 vorticity maxima and positive QGPV anomalies, while anticyclones are characterized by relative
 191 vorticity minima and negative QGPV anomalies.

$$192 \quad q''_{\zeta} = \frac{1}{f_0} \nabla^2 \phi'' \quad (2)$$

193 The vertical gradient of geopotential is related to temperature, T , through the hydrostatic
 194 relationship (Eqn 3). As a result, QGPV is also proportional the vertical change of temperature
 195 (and temperature anomalies) and therefore to atmospheric stability, with stability maxima
 196 corresponding to positive QGPV anomalies and vice versa (Eqn 4).

$$197 \quad \frac{\partial \phi''}{\partial p} = -\frac{R}{p} T'' = -\frac{R}{p} \left(\frac{p}{p_o}\right)^\kappa \theta'' \quad (3)$$

$$198 \quad q''_{st} = f_o \frac{\partial}{\partial p} \left(\frac{1}{\sigma} \frac{\partial \phi''}{\partial p} \right) \quad (4)$$

199 As such, regions in which temperature decreases rapidly with height are characterized by
 200 reduced stability and QGPV minima. Anywhere temperature (or a temperature anomaly)
 201 increases with height (or decreases less rapidly), is, conversely, associated with enhanced
 202 stability and QGPV maxima.

203 Bretherton (1966) showed that surface potential temperature (θ) anomalies could be
 204 considered as QGPV anomalies, and in particular that surface warm (cold) anomalies act as
 205 cyclonic (anticyclonic) QGPV anomalies. We include the model-output T''/θ'' anomalies as a
 206 Neumann boundary condition at the lower boundary (1000 hPa) via Eqn 3, and solve for the
 207 height field without any interior QGPV values, to determine the nonlocal response to the 1000
 208 hPa temperature anomalies produced by snow removal. The resultant geopotential anomaly shall
 209 be referred to as ϕ''_θ , and represents the balanced, troposphere-deep height response to the
 210 surface θ'' anomaly.

211 Holopainen and Karola (1991) demonstrated that one can partition QGPV anomalies in
 212 various ways, including inversion of the relative vorticity, stability and surface temperature
 213 components separately or inversion of anomalies within different vertical layers. For our
 214 purposes of isolating the surface temperature impact on the circulation, we calculated the QGPV
 215 anomalies associated with surface temperature anomalies, relative vorticity and stability

216 separately. We then determined the nonlocal impact each of these QGPV anomalies has on the
 217 circulation by inverting each anomaly separately, to retrieve its associated geopotential height
 218 fields (Eqn 5). Inversion was performed using an iterative successive overrelaxation technique.

$$219 \quad z'' = z''_{\theta} + z''_{\zeta} + z''_{st} = \frac{1}{g} \left(\phi''_{\theta} + \mathcal{L}^{-1}(q''_{\zeta}) + \mathcal{L}^{-1}(q''_{st}) \right) \quad (5)$$

220 In this manner, we were able to test our hypothesis regarding the suspected impact of removing
 221 snow on the height field near developing cyclones in the two cases examined. There is
 222 substantial cancellation between the surface temperature and stability response (which we
 223 explore in Section 3), so for brevity we consider these terms as a net temperature/stability height
 224 anomaly, $z''_T = z''_{\theta} + z''_{st}$, in some of the following analysis.

225 **3. Results**

226 Two cases were selected for investigation in this study, based upon their differences in time
 227 of year, origin, and trajectory with respect to the snow boundary. The first case examined was a
 228 typical Alberta Clipper that developed in northwesterly flow in early March 2005, crossing from
 229 north to south of the snow line during its evolution. The second was a lee-cyclogenesis case that
 230 developed east of the Rockies and propagated northeastward thereafter, crossing from south to
 231 north of the snow boundary. The immediate effect of snow removal (ie, occurring within one
 232 week following removal) in the two cases is shown in Fig. 1.

233 Regions of warm 1000 hPa temperature anomalies are observed in both cases and are broadly
 234 collocated with the area over which snow was removed. For the March 2005 case, the snow line
 235 ran northwest to southeast over the continental United States, a shape which is imitated in the
 236 90th percentile removal simulation snow line located farther north (Fig. 1a). The 1000 hPa warm
 237 anomalies developed over the removal of snow and were strongest over the upper Midwest and

238 southern Canada. The anomalies extend farther south than the area of snow removal, presumably
239 a result of mixing and advection of these anomalies by the circulation.

240 The January 1996 case exhibited a snow boundary which cut more directly west-east across
241 the continent, and in this case the temperature anomalies were characterized by three local
242 maxima over Nevada, the Great Plains, and southern Ontario (Fig. 1b). In both cases weak
243 negative height anomalies accompanied the warm temperature anomalies at 1000 hPa, consistent
244 with the notion that a surface warm anomaly produces a cyclonic QGPV/height anomaly.

245 *3.1 March 2005 Case*

246 The cyclone in this case began as a depression aligned along a region of strong
247 baroclinicity on 6 March which subsequently slid southwestward and amplified one day later
248 over Wisconsin (Fig. 2a-b). By that time the region of strongest baroclinicity was located just
249 north of the snow line, and the cyclone tracked roughly along the snow line as it propagated and
250 amplified. The cyclone weakened slightly on the 8th (Fig. 2c), subsequently deepening rapidly
251 (likely aided by ingestion of warm, moist air from over the Atlantic Ocean) as it propagated to
252 the northeast on 9 March (Fig. 2d). By this time the cyclone also exhibited a well-developed
253 thermal structure including a prominent cold front.

254 In the 90th percentile simulation, negative z'' anomalies developed near the surface just to
255 the east of where the cyclone began to develop on the 6th, over the region of snow removal and
256 farther to the south as well (Fig. 3a). The negative height anomalies strengthened thereafter,
257 overlapping with the cyclone center (and therefore deepening the height minimum of the
258 cyclone) on the 7th and 8th (Fig. 3b-c). Regions of positive height anomalies developed on 8
259 March, near the modified snow boundary, strengthening on the 9th in the cyclone's northwest
260 quadrant (Fig. 3d). Supporting our initial hypothesis, positive temperature anomalies were

261 roughly collocated with the negative height anomalies on 6-7 March (Fig. 4a-b). Later in the
262 cyclone lifecycle, however, the direct relationship between the temperature and height anomalies
263 weakens. By 8 March, and increasingly by 9 March, the correspondence between the temperature
264 and height anomalies is rather poor, with the warm anomalies remaining in the area of snow
265 removal, while positive height anomalies developed over much of eastern Canada over the snow-
266 covered region and negative height anomalies formed south of the snow boundary in the
267 Midwest United States (cf. Fig. 3d, Fig. 4d).

268 Cross sections of height and temperature anomalies (z'' and T''), taken at the times and
269 locations marked in Fig. 4b,d, indicate that on 7 March the 1000 hPa negative height anomaly
270 observed over the cyclone center extended only to 800 hPa, at which point the sign of the height
271 anomalies reversed to positive north of 45°N. (Fig. 5a). The surface warm anomaly is similarly
272 shallow, with a very weak temperature response in the mid and upper troposphere (Fig. 5c). Two
273 days later on 9 March, the negative height anomaly at the surface has weakened substantially,
274 while a stronger positive height anomaly has developed through much of the troposphere, at
275 some points extending all the way to the surface, such as at 50°N (Fig. 5b). The surface warm
276 anomaly observed on 7 March has weakened in magnitude as well, and now extends to about
277 500 hPa, tilting slightly northward with increasing altitude (Fig. 5d). A negative temperature
278 anomaly located from 200 – 300 hPa developed by this time, located just above the maximum in
279 the positive height anomaly.

280 It therefore appears that early in the cyclone lifecycle, the removal of snow enhanced the
281 cyclonic circulation near the surface. Later, this effect weakened as it was negated by a broad
282 increase in heights above the surface. Upper-tropospheric cooling is observed from 200-300 hPa
283 (consistent with presence of the height anomalies that are decreasing with height, Eqn 3)

284 revealing that, although weak, changing the lower boundary had an impact all the way to the
285 tropopause. The structure of the height response to snow removal on 7 March resembles the
286 Saharan heat low, a warm-core low pressure center that is strongest near the surface and
287 transitions to an upper-level anticyclone near 700 hPa (Lavaysse et al. 2009). Heat lows are
288 surface-driven, which may explain why their structure resembles the height response to snow
289 removal. The anticyclonic anomaly subsequently strengthened over time as observed on 9
290 March, at some locations extending to the surface.

291 Cross sections of the height fields attained associated with the combined temperature term
292 ($z_T'' = z_\theta'' + z_{st}''$) and relative vorticity components of the QGPV indicate that, as suspected, the
293 temperature term is responsible for the majority of the strong, shallow height anomaly observed
294 on 7 March (Fig. 6a-b). Above 800 hPa, the temperature and vorticity components both
295 contribute to positive height anomalies north of 45°N, while the vorticity component produced
296 negative anomalies to the south (Fig. 6c). Overall, the patterns of the height responses from z_T''
297 and z_ζ'' are notably different, with the temperature contribution displaying strong variations with
298 height, meaning it is overall baroclinic, while the relative vorticity contribution is more constant
299 with height and thus overall barotropic. Further partitioning the temperature term into
300 contributions from static stability and the surface temperature anomaly illustrates the strong
301 cancellation between these two terms (Fig. 7). The warm 1000 hPa temperature anomaly is
302 treated as a positive QGPV anomaly, inducing a cyclonic height anomaly as anticipated (Fig.
303 7a). The vertical structure of a positive temperature anomaly that decreases with height increases
304 the environmental lapse rate, reducing the stability and therefore producing a negative QGPV
305 anomaly. Correspondingly, inversion of q_{st}'' produces an anticyclonic height anomaly (Fig. 7b).
306 The sum of these two opposing aspects related to temperature and stability indicates that, at this

307 time and location, the cyclonic effect of the surface temperature anomaly is just slightly stronger
308 than the anticyclonic anomalies produced by the stability term, leading to a net negative anomaly
309 at the surface (Fig. 7c). Above 700 hPa, the stability influence is stronger and positive height
310 anomalies result (Fig. 7c and Fig. 6b, which both show z''_T but at different contour intervals).
311 Similar cancellation was observed by Holopainen and Kaurola (1991) using a prescribed surface
312 temperature and vertical temperature distribution, although the cancellation occurred higher in
313 the troposphere near 500 hPa.

314 Two days later on 9 March, the cyclonic 1000 hPa height anomaly over the cyclone center
315 weakened, due to a weaker negative anomaly associated with the z''_T term (Fig. 8a-b).
316 Simultaneously, the z''_ζ term contributed more strongly to the height field, producing positive
317 height anomalies throughout most of the troposphere, with maxima from 300-400 hPa from 35-
318 45°N, and from 800-1000 hPa at 50°N (Fig. 8c). Overall the height response appears more
319 dominated by the relative vorticity contribution to development, in contrast to the 7 March cross
320 section in which the surface temperature effect was strongest.

321 The influence of the surface warm anomaly produced by removing snow therefore appears to
322 incite a direct effect observed early in the cyclone lifecycle, which deepens the developing
323 cyclone. As the cyclone matures, however, the relative vorticity field produces an anticyclonic
324 anomaly that extends to the surface and weakens the surface cyclone in its northwest quadrant
325 (Fig. 3d). Thus while the direct response to the warm surface anomaly produced by removing
326 snow acts according to our initial hypothesis, the response in the middle and upper troposphere
327 induced by the vorticity response to snow removal also influences the development of the surface
328 cyclone.

329 *3.2 January 1996 Case*

330 The January 1996 cyclone developed predominantly south of the snow line, in contrast to
331 the March case which originated north of the snow line and propagated southeastward across it.
332 The January case also developed in the wake of a predecessor cyclone, which was not the case
333 for the March event. On 25 January, the cyclone was a small depression located in the central
334 United States just south of the snow boundary and in a broad region of baroclinicity (Fig. 9a).
335 The system propagated eastward over the next two days, its height minimum crossing to just
336 north of the snow boundary on 27 January (Fig. 9b-c). At this time the cyclone also displayed a
337 typical thermal structure including a warm sector, warm and cold fronts. One day later, the
338 cyclone continued to deepen and also expanded notably in its horizontal extent, with its center
339 located over the snow boundary in eastern Maine (Fig. 9d).

340 As in the previous case, negative 1000 hPa height anomalies result from the removal of
341 snow, located over and south of the region where the snow was removed in the 90th percentile
342 simulation (Fig. 10). On 25 January, positive height anomalies were located north of the
343 modified snow boundary over eastern Canada, over the northern portion of the predecessor
344 cyclone (Fig. 10a). From January 25-26 negative height anomalies developed to the east of the
345 developing cyclone in the central US, with weakly negative anomalies located over the cyclone
346 center (Fig. 10a-b). By 26 January, the positive anomalies observed over eastern Canada a day
347 earlier had either weakened or propagated out of the model domain, along with the predecessor
348 cyclone. On 27 January a strong couplet of negative and positive anomalies developed,
349 straddling the amplifying cyclone located over Michigan, whose center was now located directly
350 over the region of snow removal (Fig. 10c). The overall effect of removing snow in this case
351 appears to have encouraged development of the system farther to the east than where it was
352 observed, given the consistent presence of negative anomalies to the east of the cyclone

353 minimum from 25-27 January. By 28 January, the positive height anomalies west of the cyclone
354 center on the 27th had expanded and appeared to have been advected southeastward by the
355 cyclonic circulation of the system on its western edge (Fig. 10d). A region of negative height
356 anomalies is observed north of the cyclone center, having weakened substantially compared to
357 one day prior. The prevalence of negative height anomalies early in the cyclone lifecycle, which
358 transitions to a mix of positive and negative anomalies when the cyclone matures, is a common
359 element between the two cases, while the exact position of the anomalies with respect to the
360 cyclone center differs.

361 On 25 January, surface warm anomalies were roughly collocated with the negative height
362 anomalies where snow was removed, as in the March case (Fig. 11a). Thereafter, however, a
363 direct correspondence between the anomalous temperature and height fields is not apparent,
364 with, for instance, very strong warm anomalies located northwest of the cyclone on 26 January,
365 where only weakly negative or neutral height anomalies were observed (cf. Fig. 11b, Fig. 10b).
366 Warm anomalies remained within the region of snow removal over the Great Plains and upper
367 Midwest through 28 January, while the height anomalies underwent a substantially different
368 evolution as the cyclone amplified and propagated eastward. This behavior is suggestive of a
369 stronger influence of the stability and relative vorticity contributions to the height field in this
370 case, which obscured the correspondence between surface temperature anomalies and height
371 anomalies observed more clearly in the March 2005 case. We note that there is no *a priori* reason
372 to expect a direct correspondence between the height and surface temperature fields, but that the
373 presence of such a relationship was suspected to be characteristic of the impact of snow removal
374 on the circulation as suggested by Fig. 1.

375 On 25 January, the negative height anomalies and warm anomalies observed at 1000 hPa
376 were strongest near the surface and gradually weakened with altitude, though not as rapidly as
377 observed on 7 March in the previous case (cf. Fig. 12a,c, Fig. 5a,c). The height anomalies
378 changed sign to positive near 600 hPa, peaking in strength at 300 hPa. Three days later on 28
379 January, the height response over the cyclone center (located at 45°N) reversed, with positive
380 anomalies now observed south of 50°N in the lower troposphere (Fig. 12b). The temperature
381 anomaly pattern had also evolved into a broad, weak cold anomaly located near 40-45°N at the
382 surface, tilting northward with altitude to about 400 hPa (Fig. 12d). Only a small remnant of the
383 previously strong surface warm anomaly remained, centered just north of 45°N. QGPV inversion
384 will investigate which terms contributed to this dramatic change in the height anomalies.

385 Cross sections of the z''_T and z''_ζ contributions to the z'' field indicate that the former
386 accounted for most of the negative height anomaly in the lower-troposphere and positive height
387 anomalies in the mid-upper troposphere, as observed in the March case (Fig. 13a,b). The relative
388 vorticity contribution to the height field reinforced that induced by the temperature term,
389 particularly at upper levels (Fig. 13c). The deeper vertical extent of the warm anomaly in this
390 case compared to the March case (Fig. 12c) coincides with a deeper vertical extent of the
391 negative height anomalies from the surface into the troposphere. On 28 January, the z''_T response
392 reversed from its pattern on the 25th, and is associated with positive height anomalies in the
393 lower troposphere and negative height anomalies above 600 hPa (Fig. 14a-b). The vorticity
394 contribution to the height field had also changed and, by this time, accounted for the majority of
395 the negative height anomalies observed throughout the troposphere north of 45°N and positive
396 height anomalies at lower latitudes (Fig. 14c). In the net, the two components of the height field
397 enhance one another near 40°N to produce the positive anomalies observed at 1000 hPa. The

398 increase in the magnitude of the vorticity-induced anomalies later in the cyclone lifecycle is
399 similar to that observed in the March case, although there is little similarity in the structure of the
400 vorticity-induced height response between cases.

401 The complete sign reversal of the z_T'' anomalies over the course of the lifecycle, observed
402 only in the January case, is another notable difference between the cases (Fig. 12a,b). This
403 change could occur if the surface temperature anomaly changed *sign* from warm to cold, or if the
404 stability term dominates over the direct temperature effect through changes in the *vertical*
405 *structure* of the temperature field. While cold anomalies were observed in much of the lower
406 troposphere, anomalies at 1000 hPa were weak but positive at 45°N (Fig. 12d). Decomposing the
407 z_T'' term on 28 January reveals that the 1000 hPa temperature anomaly continued to induce a
408 negative/cyclonic z_θ'' anomaly, which was negated by a stronger, positive height anomaly
409 produced by the stability term (z_{st}'') in the lower troposphere (Fig. 15). The negative anomalies
410 produced by the surface temperature component are most likely driven by the nonlocal effect of
411 the broad warm anomalies observed to the west of the location of the cross section at 1000 hPa
412 (Fig. 11d). However, the stability term captures the vertical structure of the cold anomalies
413 observed more directly over the cyclone center (Fig. 12d), producing height rises where the
414 temperature anomalies decreased with altitude (Fig. 15b). The stability contribution is essentially
415 highlighting how a strong surface warm anomaly, or mid-tropospheric cold anomaly, increases
416 the environmental lapse rate and reduces the stability of the lower troposphere, creating a
417 negative QGPV anomaly and a positive height anomaly. How the removal of snow led to a cold
418 anomaly over the cyclone during its mature phase is not immediately clear, and suggests that
419 snow removal can lead to a variety of indirect and potentially opposing effects, likely related to
420 differences in the advection of temperature and vorticity between simulations.

421 **4. Discussion and Conclusions**

422 We have investigated the short-term atmospheric response to a northward-shifted snow
423 boundary during boreal winter for two cyclogenesis cases selected for their differences regarding
424 position relative to the snow line, time of year and origin. We found that the opposing effects of
425 a surface warm anomaly, which simultaneously produces a cyclonic QGPV anomaly and a
426 negative static stability anomaly, heavily influenced the height response near the surface. Our
427 results are consistent with those of Elguindi et al. (2005), who found that increasing snow cover
428 over the Great Plains weakened weather systems and enhanced lower-tropospheric stability.
429 Here, we posed the opposite problem and found an opposite result, with stronger surface cyclone
430 minima and reduced static stability.

431 In both cases investigated, the overall impact of snow removal early in the cyclone lifecycle
432 involved production of negative height anomalies which deepened the surface feature, while at
433 upper levels positive height anomalies developed above the surface warm anomalies. The
434 structure of the temperature and height fields in the nascent stage of the cyclone lifecycle in both
435 cases is similar to the structure of ‘thermal lows’ that often develop over arid regions in the
436 subtropics (Ramage 1971; Rowson and Colucci 1992). Thermal lows develop from strong
437 surface heating and have a non-frontal cyclonic circulation, and are most commonly confined to
438 below 700 hPa, with the circulation weakening and often becoming anticyclonic higher in the
439 troposphere (Petty 2008), as observed in these two cases.

440 As the relative vorticity contribution to heights strengthened later in the cyclone lifecycle, the
441 height response in both cases involved development of positive height anomalies west of the
442 surface cyclone center (cf. Fig.3, Fig. 10). The advection of height anomalies by the circulation
443 likely assisted in generating stronger horizontal height gradients, subsequently increasing the

444 magnitude of the vorticity anomalies themselves. At upper levels, the height response near the
445 cyclone center differed. Whereas the March 2005 case was characterized by positive height
446 anomalies, the January 1996 case featured a dipole of negative anomalies north of the cyclone
447 center and positive anomalies to its south. It is likely that the upper-tropospheric differences
448 between the two cases are related to the change in the temperature structure near the cyclone
449 center. The cold temperature anomalies observed on 28 January, associated with reduced
450 thickness, would be consistent with lower heights above the temperature anomaly, producing a
451 cyclonic anomaly at upper levels. In the March case, the temperature anomaly consistently
452 contributed a cyclonic anomaly, while the vorticity term contributed an anticyclonic anomaly.
453 Despite these differences, in both cases the relative vorticity response to snow removal
454 strengthened later in the cyclone lifecycle, ultimately dominating the height response.

455 Our results are roughly consistent with what Ellis and Leathers (1998) found as well, namely
456 that the inclusion of snow cools the surface and removal warms the surface. Their study used a
457 one-dimensional snow pack model to investigate the dynamics within cold air masses, which
458 assumed temperature advection by the large-scale circulation was minimal. Our study, in
459 contrast, highlights the lifecycle-dependent evolution of the temperature response engendered by
460 removing snow. We find that the advection of the initial height response to snow removal by the
461 cyclone itself generated vorticity, which subsequently produced its own height response. We
462 therefore note that, when analyzing changes in the circulation that arise due to changing snow
463 cover, advection must be considered along with in-situ interactions between the surface and
464 overlying atmosphere.

465 Through this analysis the initial hypothesis was confirmed; namely, that a surface warm
466 anomaly would be produced by removing snow, and would lead to development of a cyclonic

467 QGPV anomaly and negative height anomaly. Somewhat unexpectedly, our analysis also
468 revealed that this effect is most notable early in the cyclone lifecycle and can be negated or
469 enhanced by the response in the vorticity field. The interplay between the temperature and wind
470 responses when the lower boundary changes is thus further elucidated, suggesting that the overall
471 response of developing cyclones to snow removal may be a small residual of two substantial but
472 opposing forcings. The surface warm anomaly, being a surrogate positive PV anomaly, serves to
473 induce negative height anomalies. As in the March 2005 case, the surface warming can
474 simultaneously lead to increased heights aloft via hypsometry. These local height increases
475 induce an anticyclonic vorticity anomaly aloft whose influence can extend back down to the
476 surface and manifest itself as opposing positive height anomalies. Alternatively, a cold anomaly
477 developed in the lower troposphere in the January 1996 case near the cyclone center, suggesting
478 that mixing and advection of air masses can oppose the surface warm anomaly initially produced
479 by removing snow.

480 In sum, the effects of removing snow on the cyclone lifecycle are observed and quantifiable,
481 but are generally transient and, even at their strongest, rather limited in magnitude and effect.
482 Large, permanent changes to cyclone intensity and trajectory due to changes in the snow
483 boundary do not seem likely when the snow removal leads cyclogenesis on daily timescales. We
484 emphasize that the long-term, nonlocal impacts of a receding snow line were not the target of
485 this analysis and could still have a large effect on the circulation, but the immediate, direct
486 effects of snow removal appear to be relatively minimal through the mitigating responses of
487 various components of the circulation. It is important to note that just two cases have been
488 analyzed in this study, with the goal of exploring the possible ways in which snow removal *could*
489 affect the cyclone lifecycle. However, statistical analysis of a larger number of cases from the

490 same model case studies reveals a relatively similar effect across all cases (Clare et al.,
491 submitted). Additionally, other features of storm evolution, including precipitation type,
492 mesoscale “snow-breeze” circulations, or cloud microphysics were not investigated, and could
493 be influenced by the snow cover change. Future work could apply the same methods employed
494 here to a larger sample of the simulations to better understand the average response of
495 midlatitude cyclones to a northward-shifted snow boundary.

496

497 **Data Availability**

498 All model outputs are being submitted to the Environmental Data Initiative (EDI) repository, and
499 the DOI/URL will be added prior to acceptance. Reviewers can access model data
500 at: <http://co2.aos.wisc.edu/data/snowcover/>.

501

502 **Acknowledgements**

503 The authors acknowledge support for this project by the University of Wisconsin Office of the
504 Vice Chancellor for Research and Graduate Education Fall Research Competition and
505 the National Science Foundation Climate and Large-Scale Dynamics program award (NSF AGS-
506 1640452). We also acknowledge technical support from the UW Advanced Computing Initiative
507 (ACI) Center for High Throughput Computing (CHTC). We would also like to acknowledge Dr.
508 Michael Notaro for assistance with model simulations.

509

510 **References**

511 Bretherton, F. B., Critical Layer Instability in baroclinic flows. *Quart. J. Roy. Met. Soc.*, **92**,
512 325-334.

513

514 Brown, R. D., 2000: Northern Hemisphere snow cover variability and change, 1915-97,
515 *Journal of Climate*, **13**, 2339-2354, doi:10.1175/1520-0442(2000)013<2339:NHSCVA>2.0.CO;2.

516

517 Brutel-Vuilmet, C., M. Menegoz, and G. Krinner, 2013: An analysis of present and future
518 seasonal Northern Hemisphere land snow cover simulated by CMIP5 coupled climate models.
519 *The Cryosphere*, **7**, 67-80, doi:10.5194/tc-7-67-2013.

520

521 Clare, R., 2018: Modelled response of extratropical cyclone cases in the great plains to
522 projected late twenty-first century snow cover extents. Masters Thesis, University of Wisconsin-
523 Madison, 79pp.

524

525 Clare R., A. R. Desai, J. E. Martin, M. Notaro, and S. J. Vavrus: Extratropical Cyclone
526 Response to Projected Reductions in Snow Extent over the Great Plains. Submitted to *J. Climate*
527 February 2020.

528

529 Elguindi, B. Hanson, and D. Leathers, 2005: The effects of snow cover on midlatitude
530 cyclones in the Great Plains. *Journal of Hydrometeorology*, **6**, 263-279, doi:10.1175/JHM415.1.

531

532 Ellis, A. W. and D. J. Leathers, 1999: Analysis of cold airmass temperature modification
533 across the US Great Plains as a consequence of snow depth and albedo. *Journal of Applied*
534 *Meteorology and Climatology*, **38**, 696-711, doi:10.1175/1520-
535 0450(1999)038<0696:AOCATM>2.0.CO;2.

536

537 Gan, T. Y., R. G. Barry, M. Gizaw, A. Gobena, and R. Balaji, 2013: Changes in North
538 American snowpacks for 1979-2007 detected from the snow water equivalent data of SMMR
539 and SSM/I passive microwave and related climatic factors. *Journal of Geophysical Research:
540 Atmospheres*, **118**(14), 7682-7697, doi:10.1002/jgrd.50507.

541

542 Holopainen, E. and Kaurola, J. (1991) Decomposing the atmospheric flow using potential
543 vorticity framework. *Journal of the Atmospheric Sciences*, 48, 2614–2625.

544

545 Klingaman, N.P., B. Hanson, and D.J. Leathers, 2008: [A Teleconnection between Forced
546 Great Plains Snow Cover and European Winter Climate](#). *J. Climate*, **21**, 2466–
547 2483, <https://doi.org/10.1175/2007JCLI1672.1>

548

549 Lavaysse, C., Flamant, C., Janicot, S. et al., 2009: Seasonal evolution of the West African
550 heat low: a climatological perspective. *Clim. Dyn.*, **33**: 313. [https://doi.org/10.1007/s00382-
551 009-0553-4](https://doi.org/10.1007/s00382-009-0553-4)

552

553 Lemke, P., J. Ren, R. B. Alley, I. Allison, J. Carrasco, G. Flato, Y. Fujii, G. Kaser, P. Mote,
554 R. H. Thomas, and T. Zhang, 2007: Observations: Changes in Snow, Ice, and Frozen Ground. In:
555 *Climate Change 2007: The Physical Science Basis. Contribution of Working Group I to the
556 Fourth Assessment Report of the Intergovernmental Panel on Climate Change* [Solomon, S., D.
557 Qin, M. Manning, Z. Chen, M. Marquis, K. B. Avery, M. Tignor, and H. L. Miller (eds.)].
558 Cambridge University Press, Cambridge, United Kingdom and New York, NY, USA.

559

560 Manabe, S. and R. T. Wetherald, 1980: On the distribution of climate change resulting from
561 an increase in CO₂ content of the atmosphere. *Journal of Atmospheric Sciences*, **37**, 99-118,
562 doi:10.1175/1520-0469(1980)037<0099:OTDOCC>2.0.CO;2.

563

564 Petty, G. W., 2008: *A First Course in Atmospheric Thermodynamics*. 337 p. Sundog
565 Publishing, Madison, WI.

566

567 Ramage, C.S. (1971) *Monsoon Meteorology*. Academic Press, New York, 296 p.

568

569 Ross, B. and J.E. Walsh, 1986: *Synoptic-Scale Influences of Snow Cover and Sea Ice*. *Mon.*
570 *Wea. Rev.*, **114**, 1795–1810, [https://doi.org/10.1175/1520-](https://doi.org/10.1175/1520-0493(1986)114<1795:SSIOSC>2.0.CO;2)
571 [0493\(1986\)114<1795:SSIOSC>2.0.CO;2](https://doi.org/10.1175/1520-0493(1986)114<1795:SSIOSC>2.0.CO;2)

572

573 Rowson, D. R. and S. J. Colucci, 1992: Synoptic climatology of thermal low-pressure
574 systems over south-western north America. *International J. of Climatology*. **12**, 529-545.

575

576 Rydzik, M. and A. R. Desai, 2014: Relationship between snow extent and midlatitude
577 disturbance centers. *Journal of Climate*, **27**, 2971-2982, doi:10.1175/JCLI-D-12-00841.1.

578

579 Sobolowski, S., G. Gong, and M. Ting, 2010: Modeled climate state and dynamic response to
580 anomalous North American snow cover. *Journal of Climate*, **23**, 785-799,
581 doi:10.1175/2009JCLI3219.1.

582
583

Modeling Center (or Group)	Institute ID	Model Name	Horizontal Res. (°lon × °lat)	No. Vertical Levels
Commonwealth Scientific and Industrial Research Organization (CSIRO) and Bureau of Meteorology (BOM), Australia	CSIRO-BOM	ACCESS1.0	1.875 × 1.25	38
National Center for Atmospheric Research	NCAR	CCSM4	1.25 × 1.0	26
Centre National de Recherches Météorologique/Centre Européen de Recherche et Formation Avancée en Calcul Scientifique	CNRM-CERFACS	CNRM-CM5	1.4 × 1.4	31
Commonwealth Scientific and Industrial Research Organization in collaboration with Queensland Climate Change Centre of Excellence	CSIRO-QCCCE	CSIRO-Mk3.6.0	1.8 × 1.8	18
NASA Goddard Institute for Space Studies	NASA GISS	GISS-E2-H, GISS-E2-R	2.5 × 2.0	40
Met Office Hadley Centre	MOHC	HadGEM2-CC, HadGEM2-ES	1.8 × 1.25	60
Institute for Numerical Mathematics	INM	INM-CM4	2.0 × 1.5	21
Atmosphere and Ocean Research Institute (The University of Tokyo), National Institute for Environmental Studies, and Japan Agency for Marine-Earth Science and Technology	MIROC	MIROC5	1.4 × 1.4	40
Max Planck Institute for Meteorology	MPI-M	MPI-ESM-LR	1.9 × 1.9	47
Meteorological Research Institute	MRI	MRI-CGCM3	1.1 × 1.1	48
Norwegian Climate Centre	NCC	NorESM1-M, NorESM1-ME	2.5 × 1.9	26

584 **Tables**

585

586

587

588

589

590 Table 1: CMIP5 models used to determine the range of likely changes in the position of the

591 snow/no snow boundary through the year 2100.

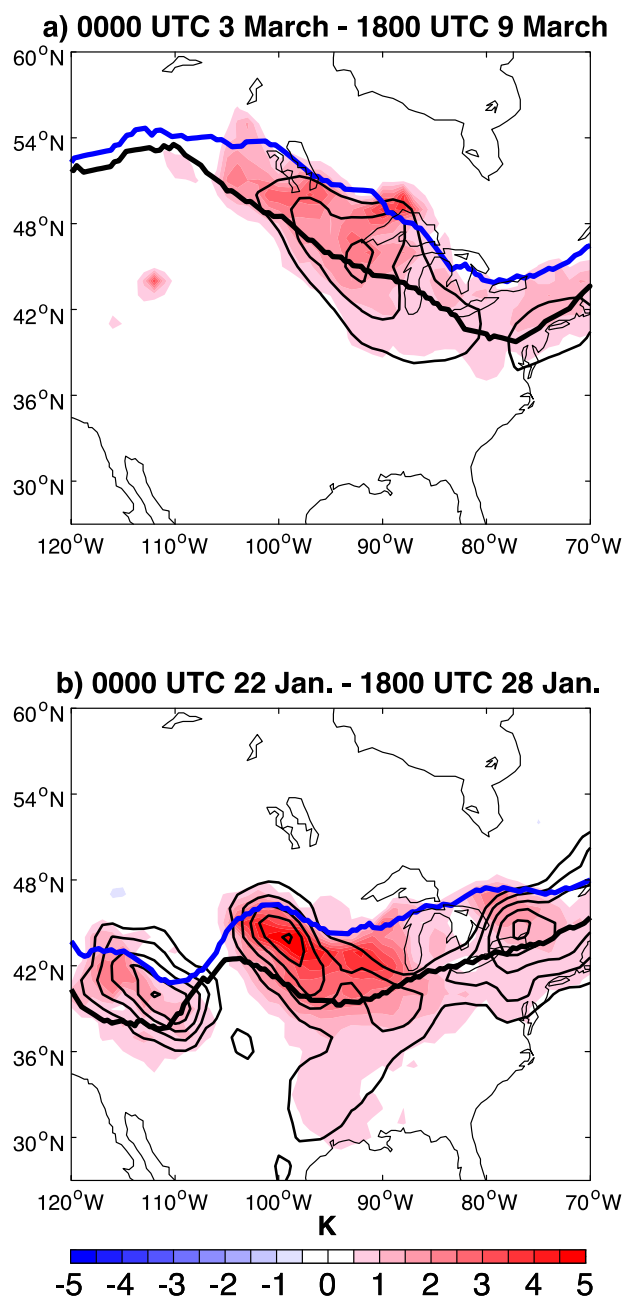
592

593

594

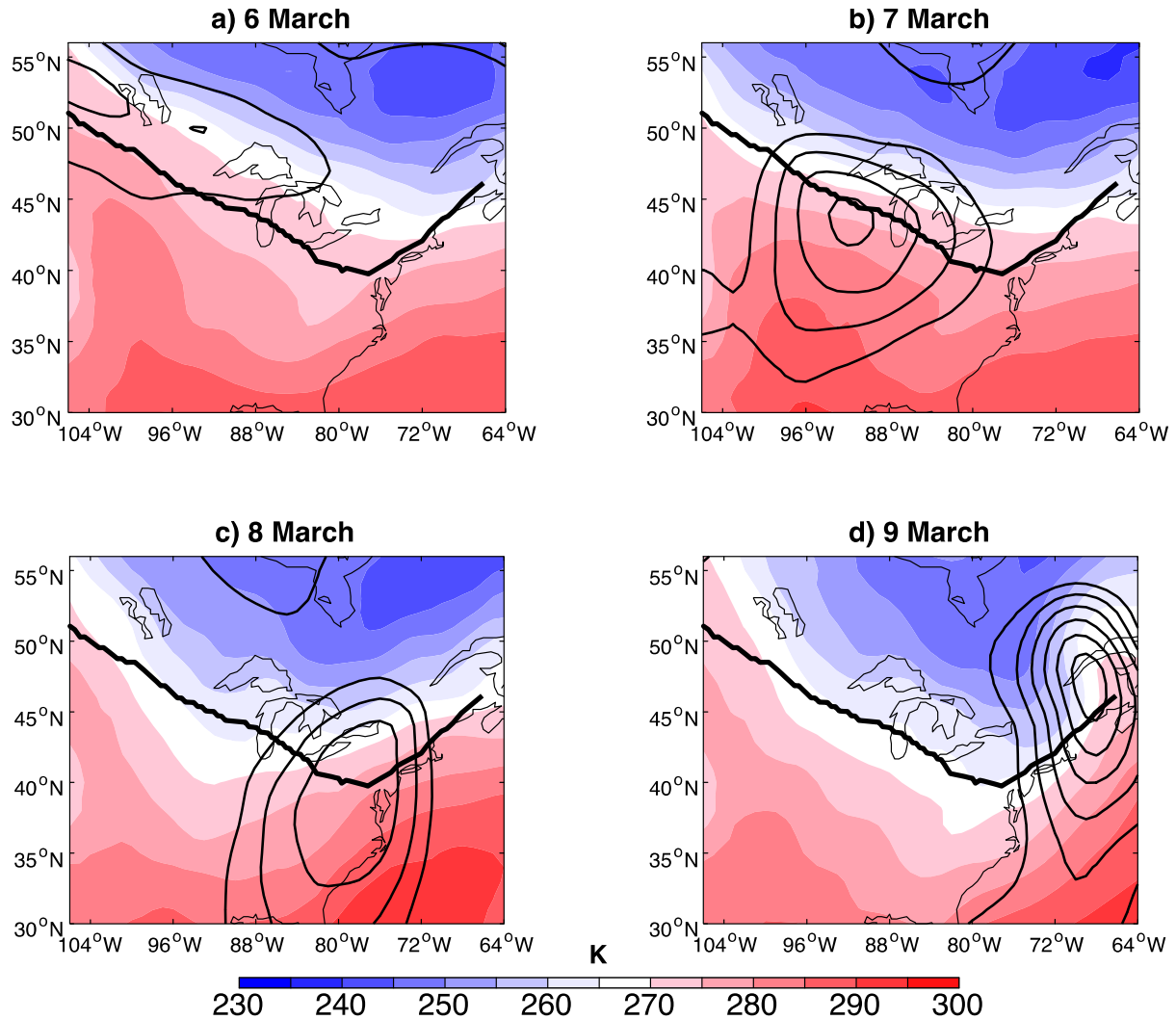
595
596
597
598

Figures



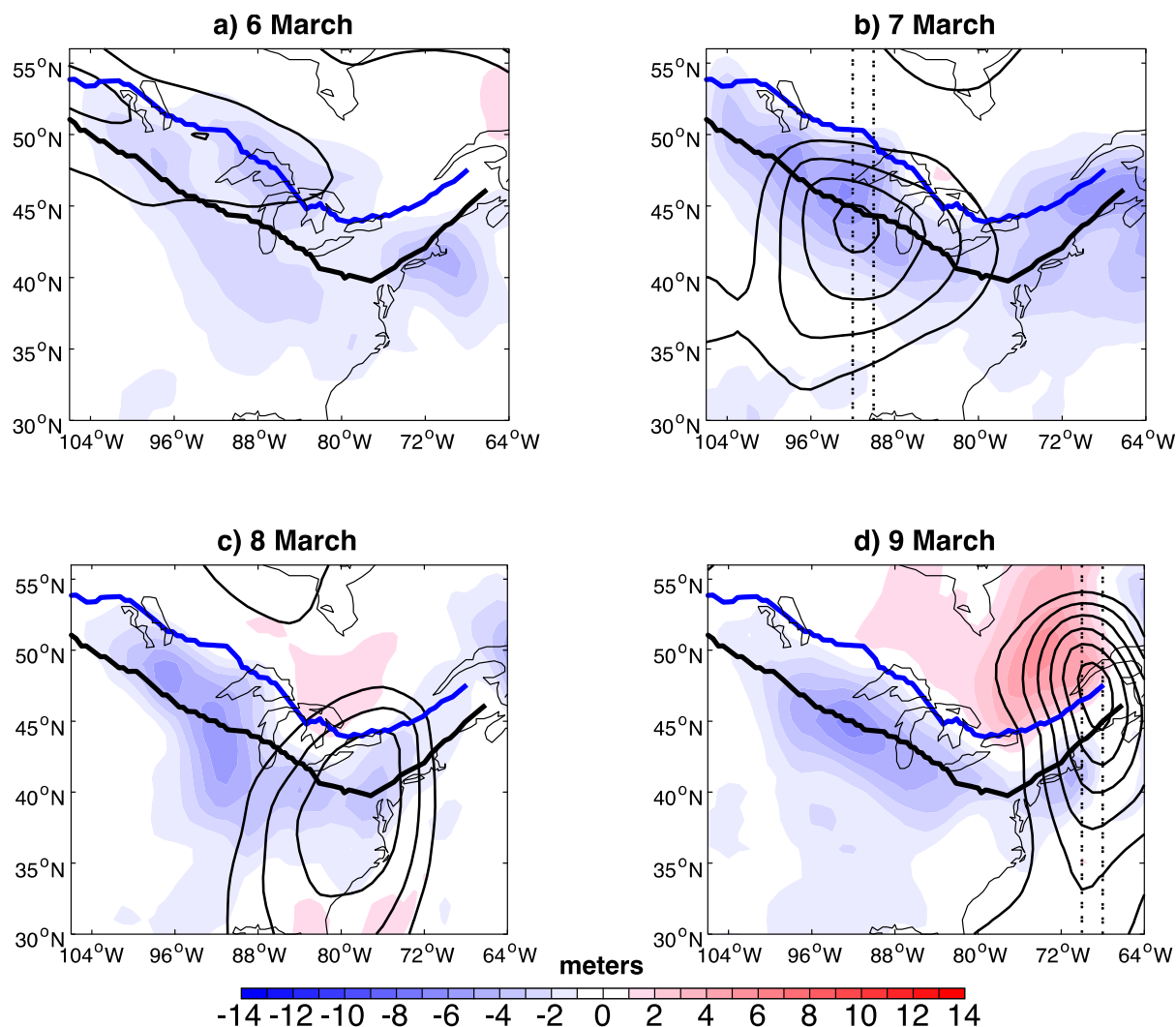
599
600
601
602
603
604
605

Figure 1: Location of snow boundary in control (bold black line), 90% removal simulations (bold blue line) including simulated 7-day average 1000 hPa temperature anomaly in the color shading and 7-day average 1000 hPa height anomalies, negative values only, beginning at -2 meters contoured every 1 meter (thin black lines), for (a) 0000 UTC 3 March – 1800 UTC 9 March 2005 and (b) 0000 UTC 22 January – 1800 UTC 28 January 1996.



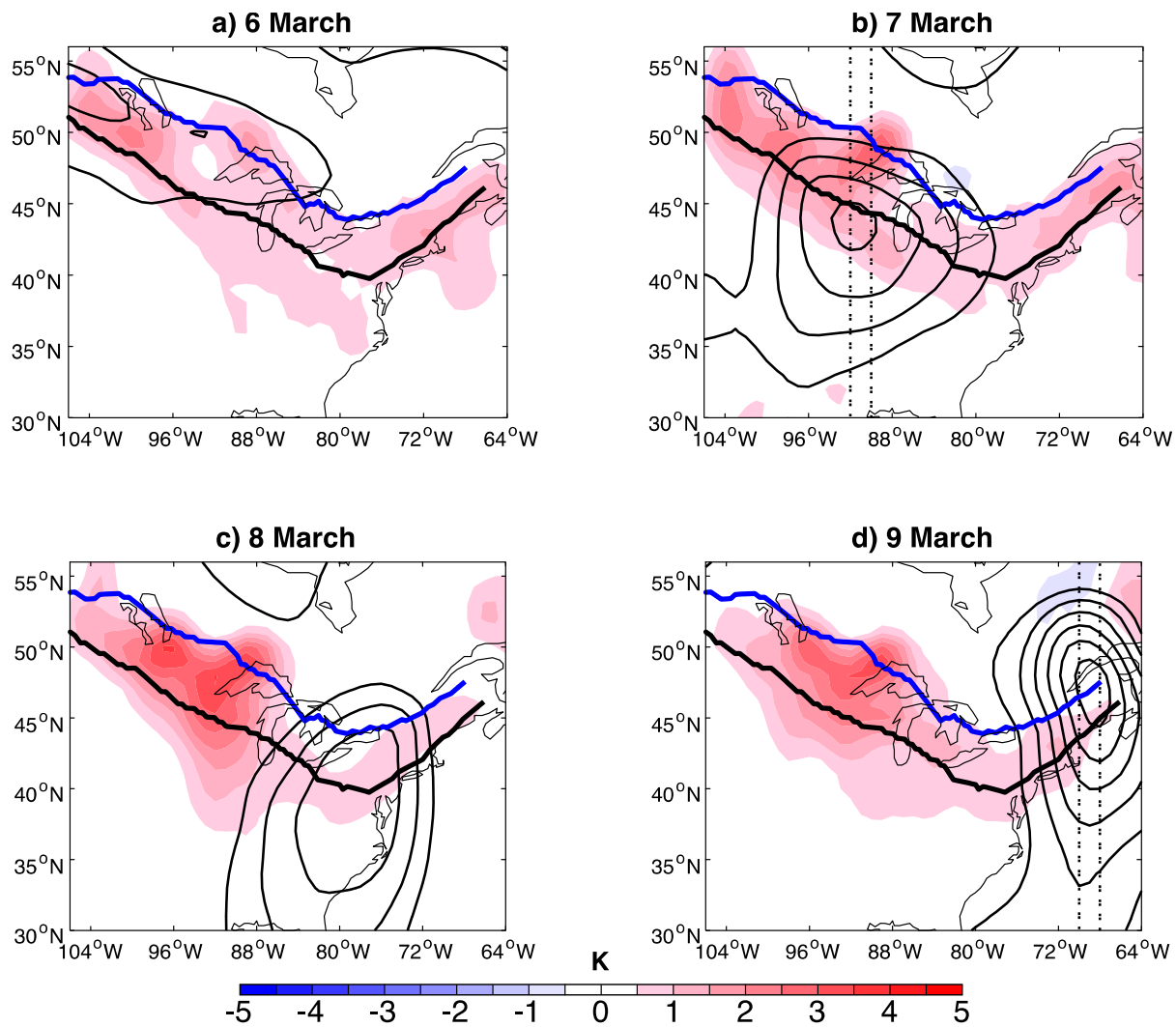
606
 607
 608
 609
 610
 611
 612

Figure 2: The color shading shows the daily mean 1000 hPa temperature, and the black thin contours show the 1000 hPa z' field (anomalies calculated with respect to the 0000 UTC 3 March – 1800 UTC 9 March average), contoured every 25 meters starting at -25 meters, negative values only, for (a) 6 March through (d) 9 March, 2005. Fields are shown for the control simulation. The thick black line marks the location of the snow line in the control simulation.



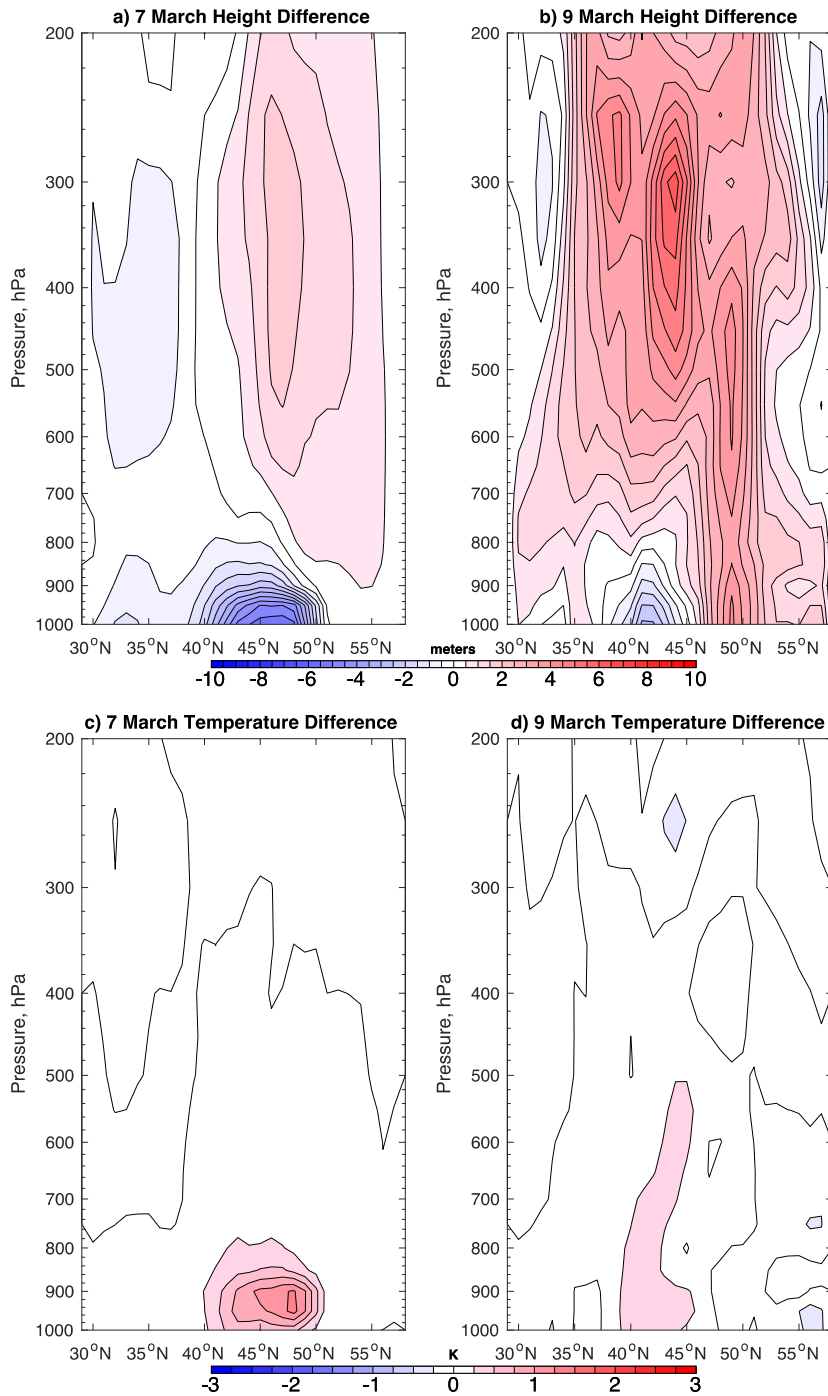
613
 614
 615
 616
 617
 618
 619
 620
 621
 622
 623

Figure 3: The color shading shows the daily mean 1000 hPa z'' field (anomalies calculated as the difference: 90th percentile simulation - Control simulation) at (a) 6 March – (d) 9 March, 2005. The thin black contours show the 1000 hPa z' field, calculated with respect to the 0000 UTC 3 March – 1800 UTC 9 March average, contoured every 25 meters starting at -25 meters, negative values only. The thick black line marks the location of the snow line in the control simulation, while the thick blue line shows the snow line in the 90th percentile snow removal simulation. The dashed lines in panels (b) and (d) mark the location of cross sections presented in Fig. 5.



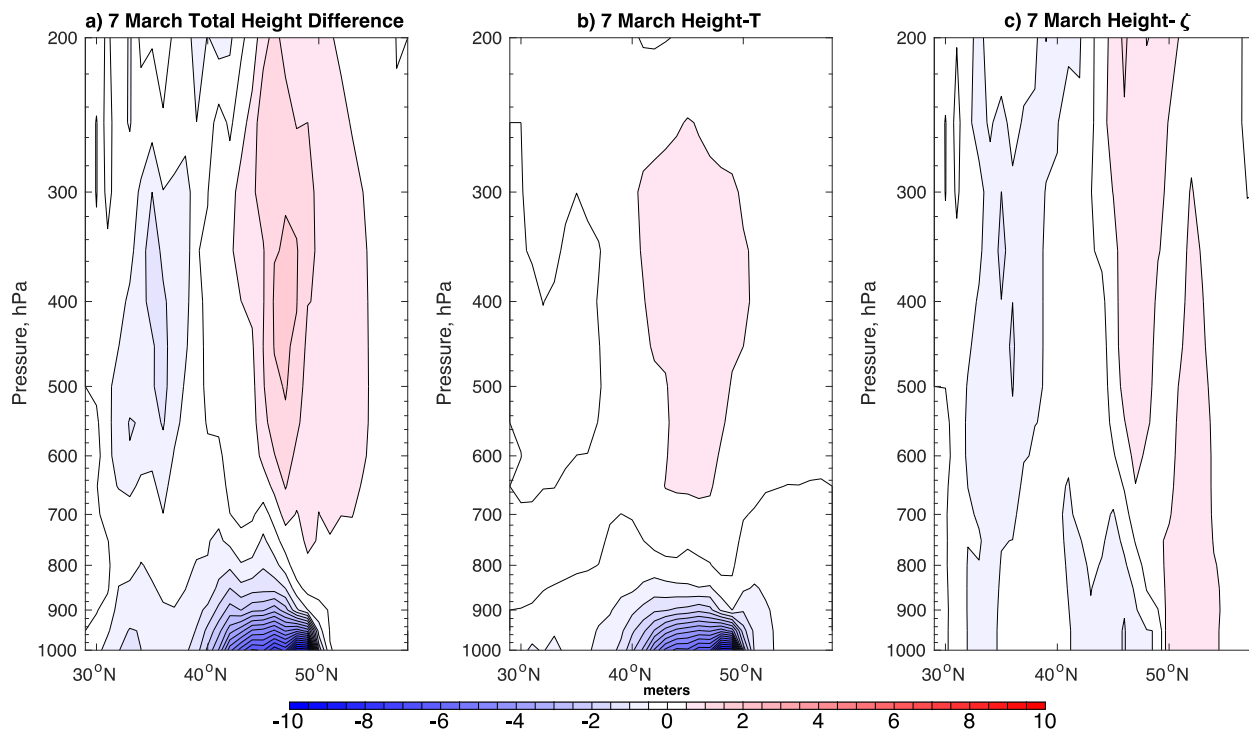
624
625
626
627
628
629
630

Figure 4: As in Figure 3 but with the color shading showing the daily mean difference in 1000 hPa T'' field.



631
632

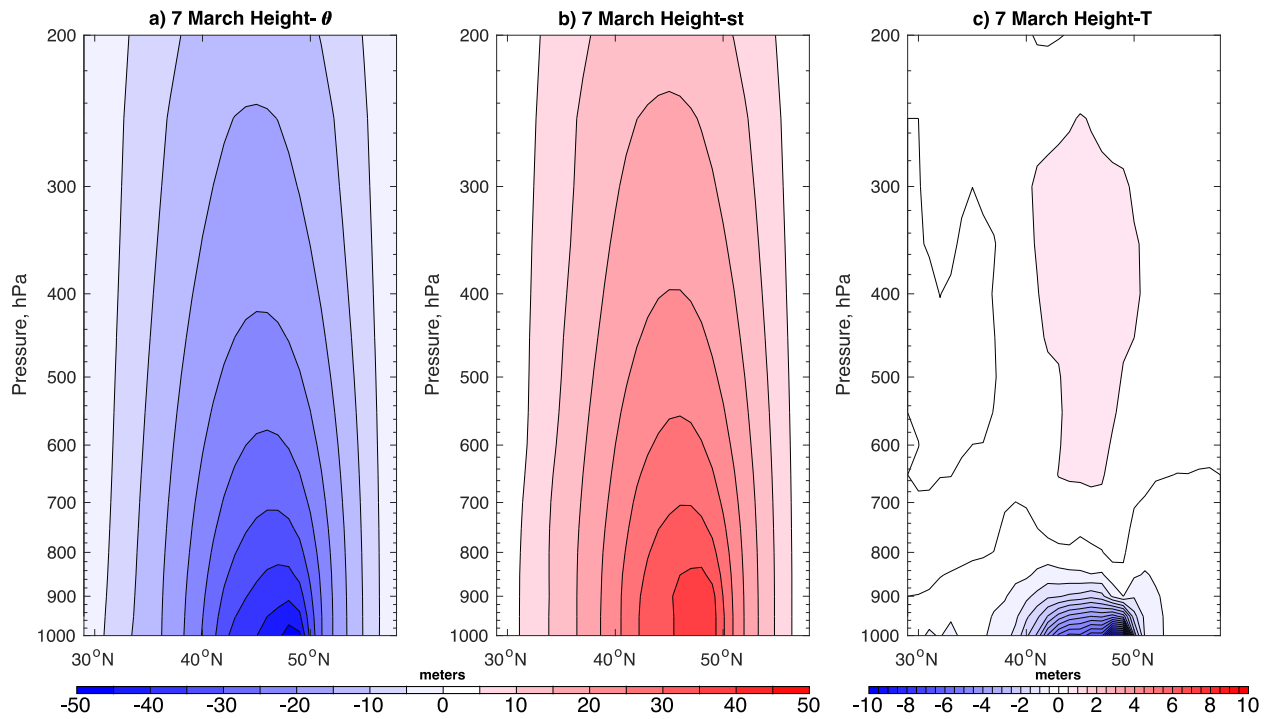
633 Figure 5: Cross sections of (a)-(b) z'' and (c)-(d) T'' taken at the locations and times shown in
634 Fig. 4b,d. The left panels show cross sections taken on 7 March averaged from 268-270°E, and
635 the right panels show cross sections taken on 9 March averaged from 290-292°E.



636
637

638 Figure 6: Cross-sections of the (a) total height change, (b) height change due to the z_T'' term, and
639 (c) height change due to the z_ζ'' term. All fields were averaged from 268-270°E (location shown
640 in Fig. 4b) from 0000 – 1800 UTC 7 March 2005.

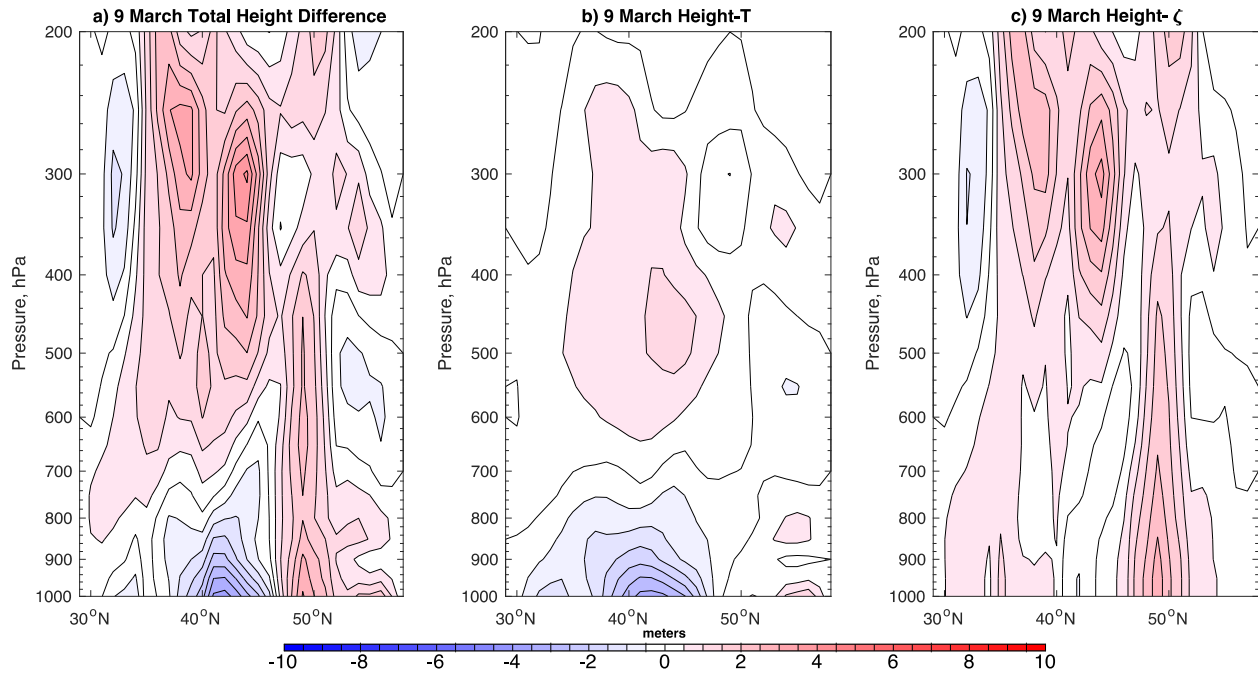
641
642
643
644
645
646
647
648



649
650

651 Figure 7: Decomposition of the z''_T field into contributions from (a) z''_θ and (b) z''_{st} on 7 March
652 2005. The net response, z''_T , is shown in panel (c). Note the change in the color scale compared to
653 Figure 6, and that panel (c) is the same field as Fig. 6b.

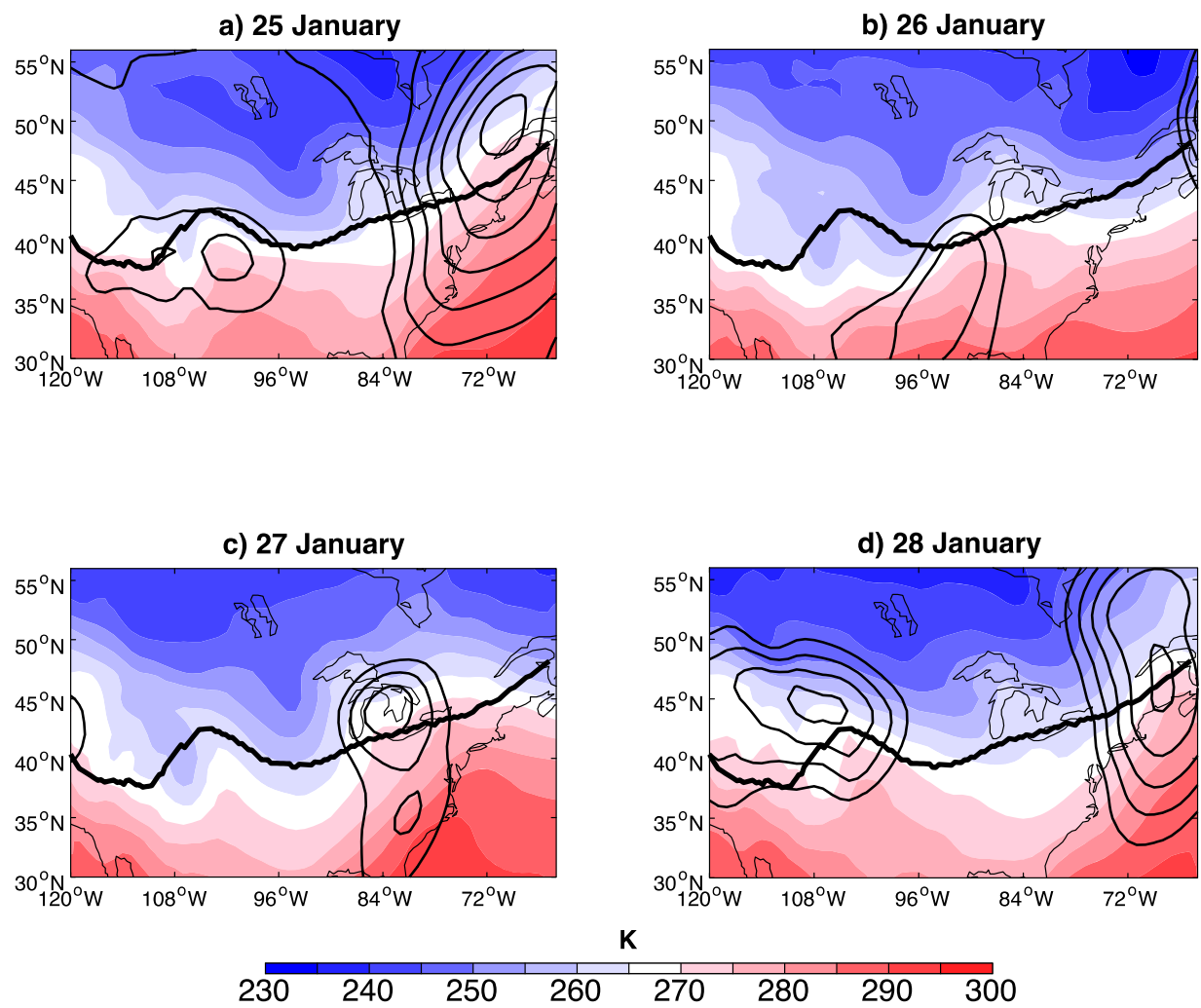
654
655
656
657
658
659
660
661
662



663
664

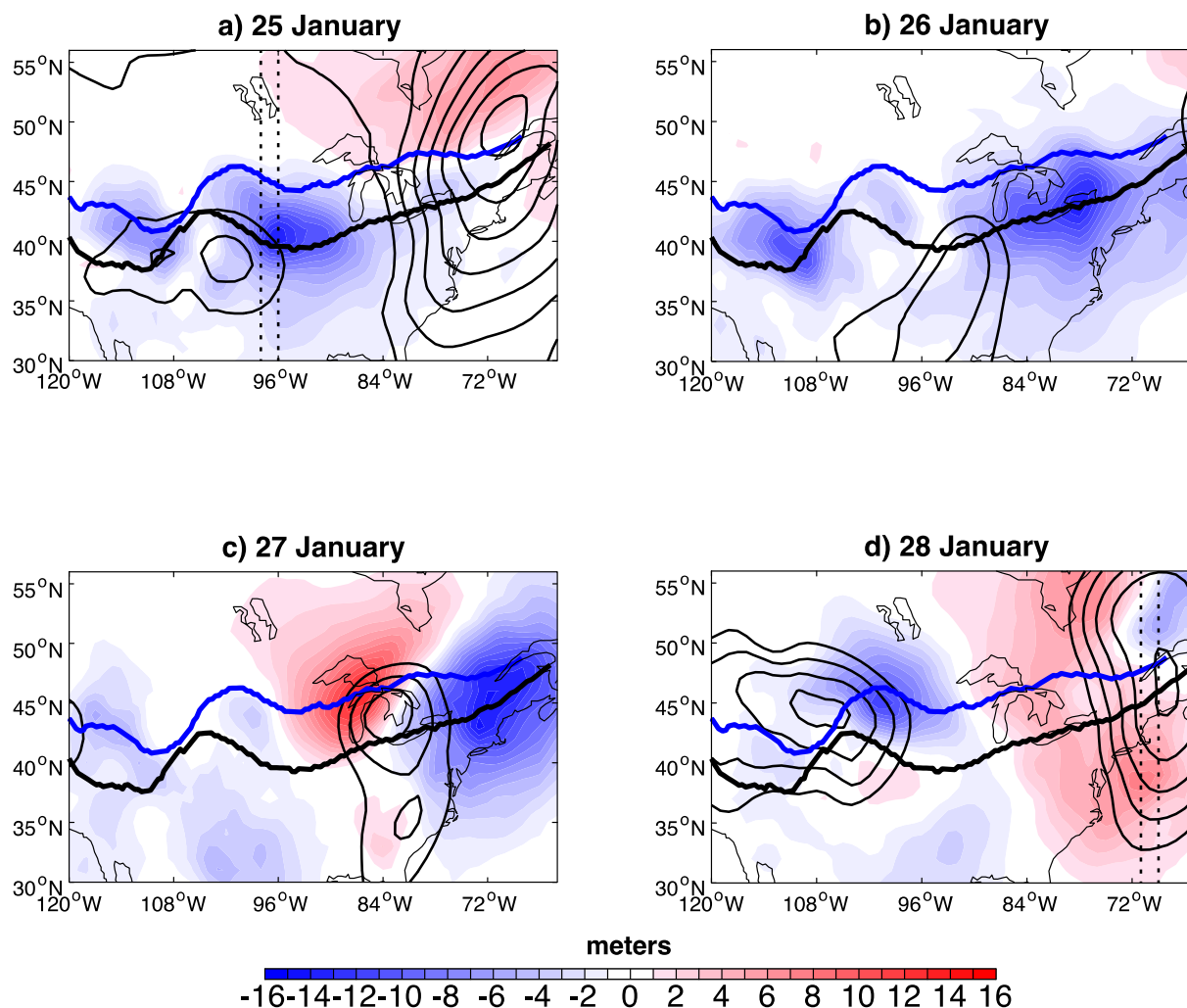
665 Figure 8: As in Fig. 6 but averaged from 0000 – 1800 UTC 9 March 2005, and over longitudes
666 290-292°E.

667
668
669

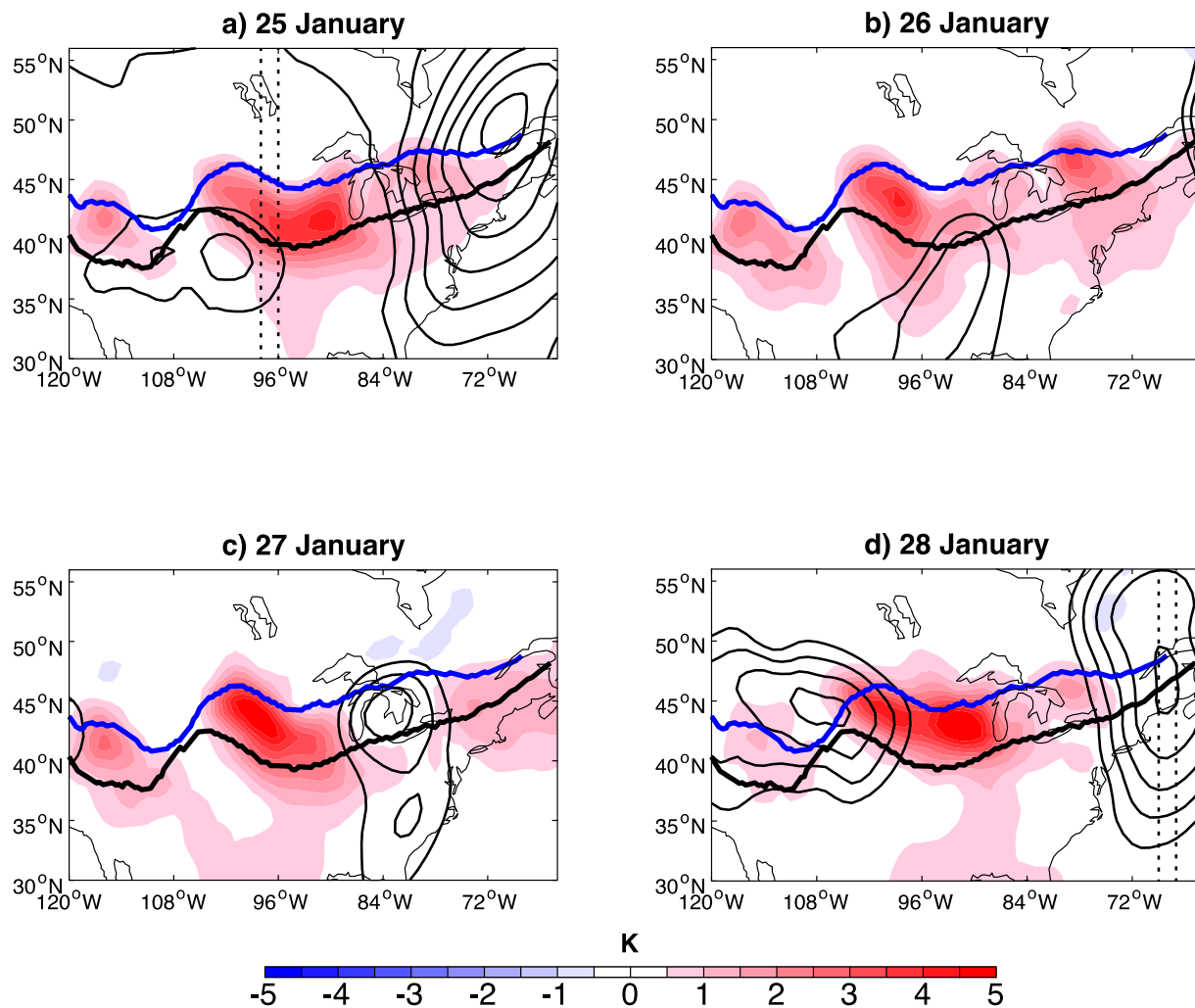


670
671
672
673
674
675
676
677
678
679
680

Figure 9: The color shading shows the daily mean 1000 hPa temperature, and the black thin contours show the 1000 hPa z' field (anomalies calculated with respect to the 0000 UTC 22 January – 1800 UTC 28 January 1996 average), contoured every 25 meters starting at -25 meters, negative values only, for (a) 25 January through (d) 28 January, 1996. Fields are shown for the control simulation. The thick black line marks the location of the snow line in the control simulation.

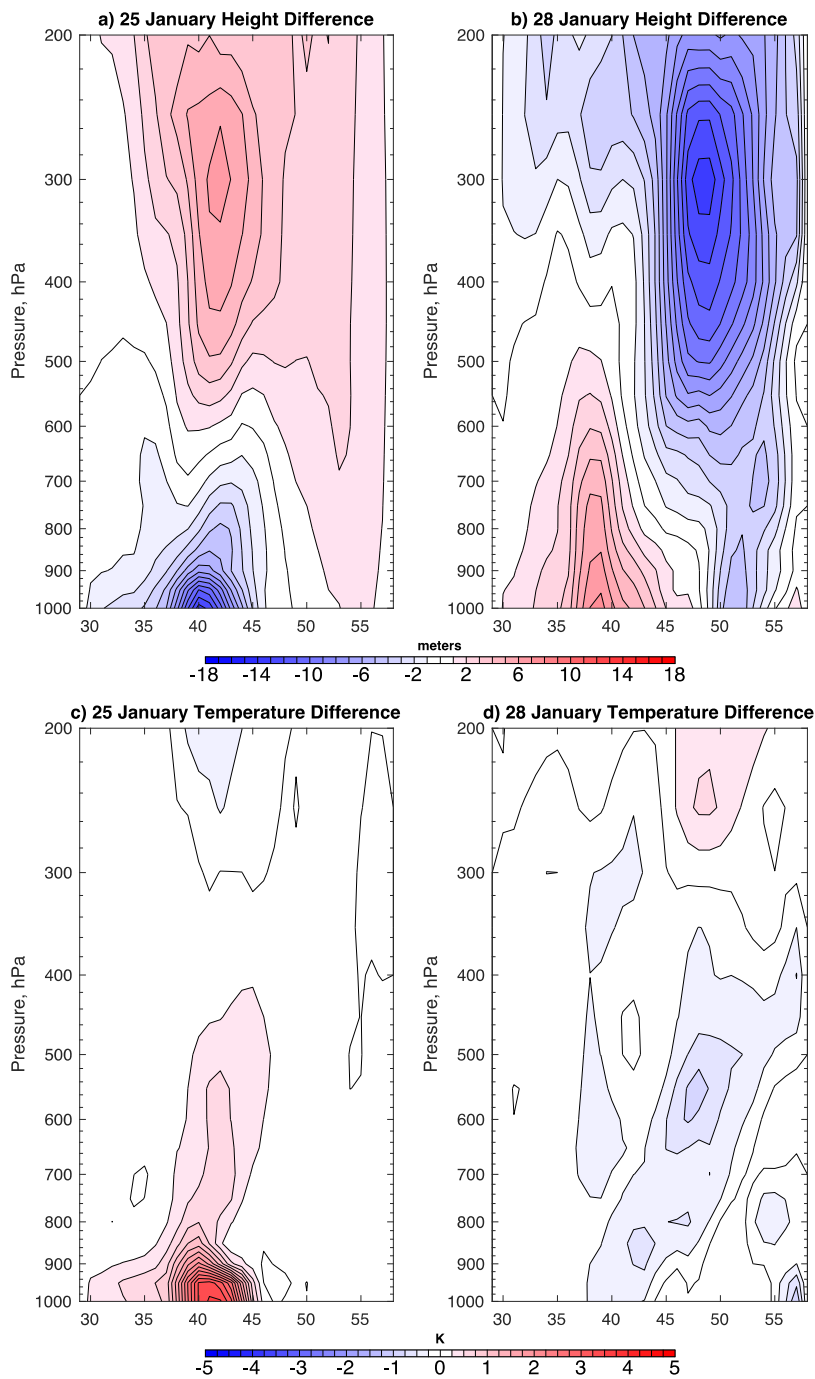


681
 682
 683 Figure 10: The color shading shows the daily mean 1000 hPa z'' field (anomalies calculated as
 684 the difference: 90th percentile simulation - Control simulation) at (a) 25 January – (d) 28 January,
 685 1996. The thin black contours show the 1000 hPa z' field, contoured every 25 meters starting at -
 686 25 meters, negative values only. The thick black line marks the location of the snow line in the
 687 control simulation, while the thick blue line shows the snow line in the 90th percentile snow
 688 removal simulation. The dashed lines in panels (a) and (d) mark the location of cross sections
 689 presented in Fig. 12.
 690
 691



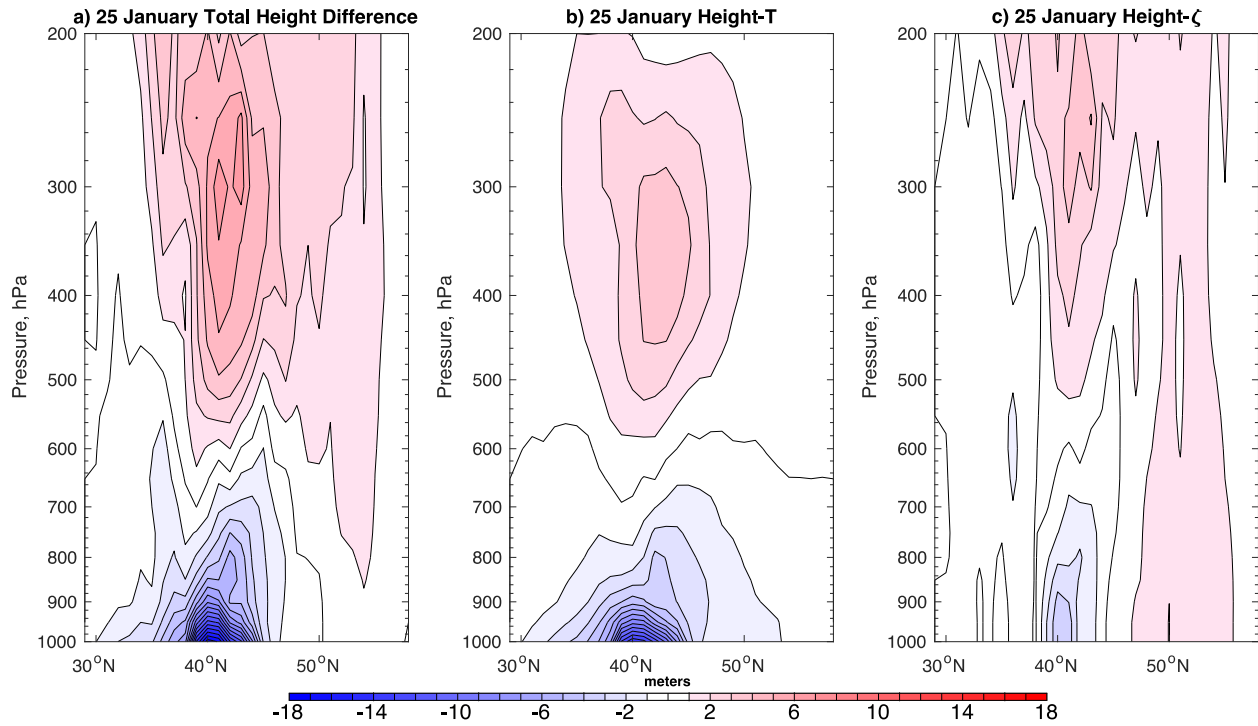
692
 693
 694
 695
 696
 697
 698

Figure 11: As in Figure 10 but with the color shading showing the 1000 hPa T'' anomalies.



699
700

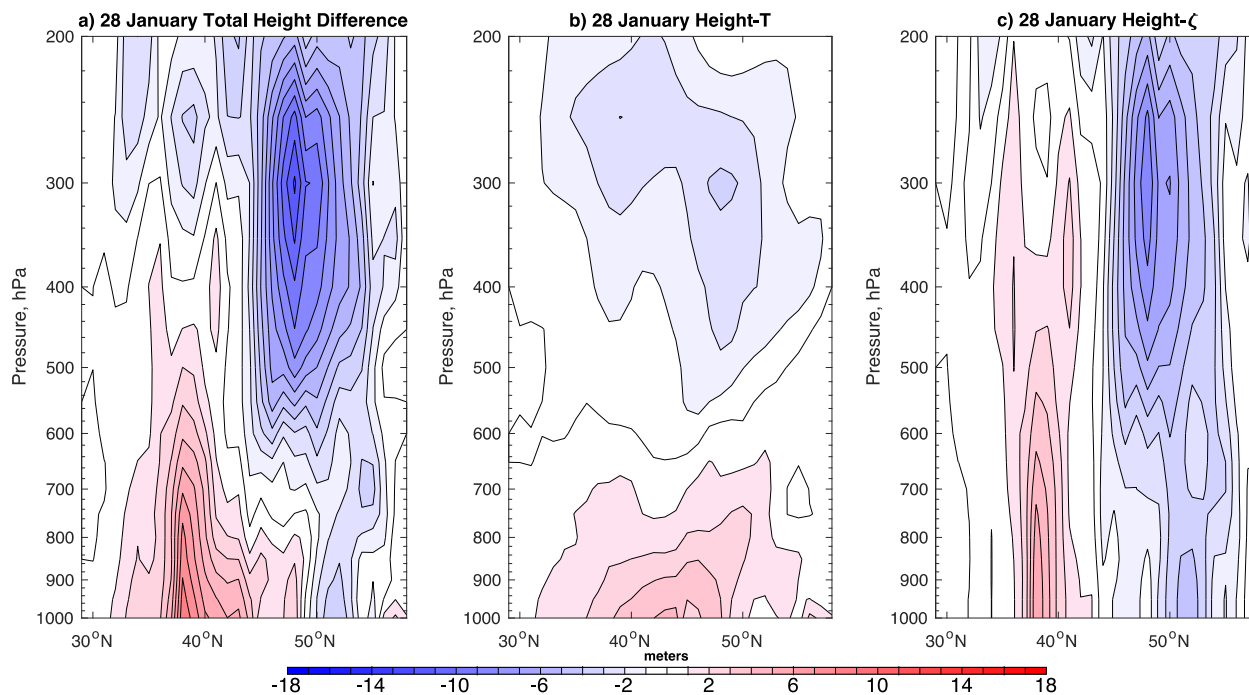
701 Figure 12: Cross sections of geopotential height (top) and temperature (bottom) averaged over
702 the locations indicated in Fig. 11 on (a), (c) 25 January and (b), (d) 28 January, 1996.



703
704

705 Figure 13: Cross-sections of the (a) total height change, (b) height change due to the z_T'' term,
706 and (c) height change due to the z_ζ'' term. All fields were averaged from 260-262°E (location
707 shown in Fig. 11a) from 0000 – 1800 UTC 25 January 1996.

708
709
710
711
712
713
714
715
716



717

718

719 Figure 14: As in Fig. 13 but averaged from 289-291°E from 0000 UTC – 1800 UTC 28 January
 720 1996.

721

722

723

724

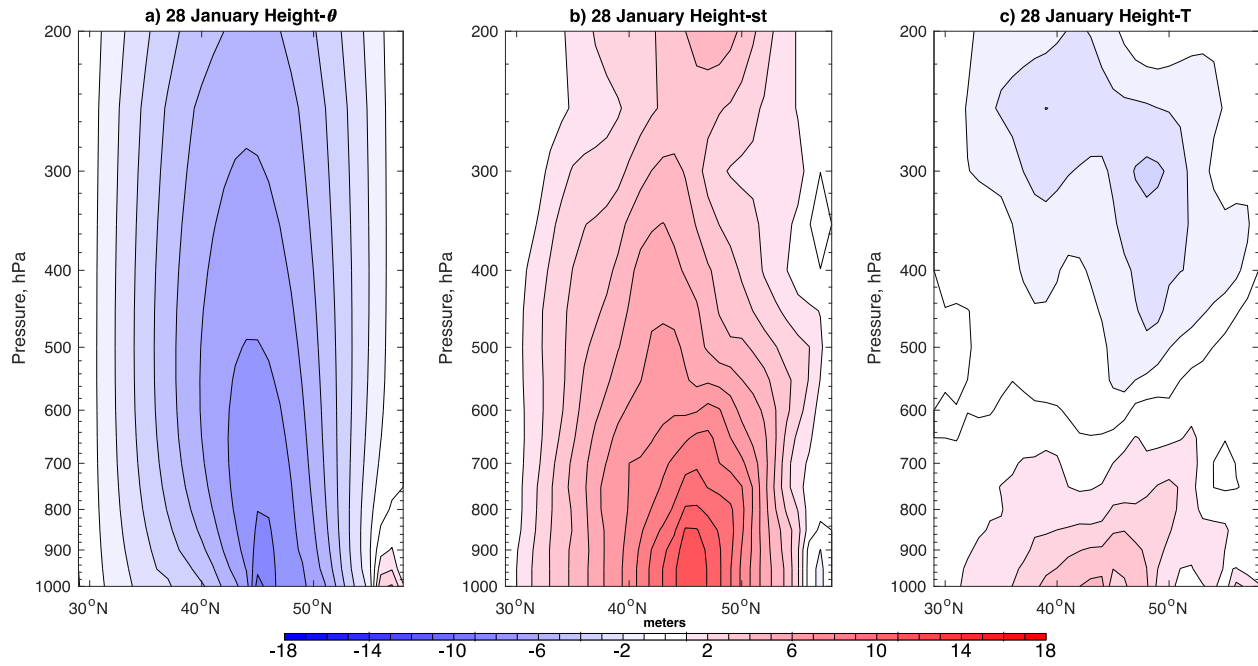
725

726

727

728

729



730
731
732
733
734
735
736
737

Figure 15: Decomposition of the z_T'' field into contributions from (a) z_θ'' and (b) z_{st}'' on 28 January 1996. The net response, z_T'' , is shown in panel (c).